RSC Advances

PAPER

View Article Online
View Journal | View Issue

Cite this: *RSC Adv.*, 2016, **6**, 112158

Autonomous movement in mixed metal based soft-oxometalates induced by CO_2 evolution and topological effects on their propulsion†

Apabrita Mallick and Soumyajit Roy*

Received 28th September 2016
Accepted 21st November 2016

DOI: 10.1039/c6ra24132h

www.rsc.org/advances

In current nanoscience, the synthesis of autonomously moving nanomotors proves to be an immediate challenge. In this work we have reported the synthesis of soft-oxometalate (SOM) based nanomotors comprising vanadium and molybdenum oxoanions which show autonomous movement in response to a chemical fuel like that of an aqueous solution of sodium bicarbonate. CO_2 produced from bicarbonate in an acidic environment created by the SOMs is solely responsible for creating the chemical potential gradient which induces motion in these nanomotors. We have explained this motion qualitatively and also shown how chemical anisotropy and size of these nanoparticles influence such autonomous motion.

Introduction

Nanomachines[1,2] play a significant role in today's nanotechnology as they can perform tailored tasks using energy. Nanomotors prove to be a step towards realisation of such nanomachines.[3,4] Nanomotors may be defined as nano scale objects which harness energy from their environment and convert it to motion and force. In nature various biological motors are present.[5] For instance, eukaryotic cells contain several powerful biomotors which convert chemical energy from hydrolysis of ATP to mechanical work.[6] Other examples of biomotors include cytoskeletal molecular motors and enzymatic motors which are involved in the processing of RNA and DNA.[7,8] Taking inspiration from these biological machines various groups across the world have started working with nano machines. The first attempt of preparing such small-scale machines was taken by Whitesides *et al.* in 2002.[9] They used Pt catalyst to propel millimetre sized plastic disks. In 2004–2005 the group of Sen, Mallouk and Ozin contributed further to this field by preparing micrometre sized motors which constituted of Pt–Au and Ni–Au bimetallic rods of length 2–3 μm.[10,11] These were chemically driven micromotors and the fuel used in these cases was primarily H_2O_2 which catalytically decomposed to form H_2O and O_2.

The motion of these nanomotors is dominated by viscous force and thermal fluctuations which are converted to Brownian motion.[12,13] In order to overcome the viscous force in low Reynold's number regime and also to induce motion in the nanomotors some form of energy input must be provided.[14] This is because of the fact that the mechanism of motion of nanoscale objects differs from that of macro objects.[15,16] A macro particle can maintain its motion for a certain period of time even without continuous supply of energy but a nanoscale object cannot continue its motion due to the dominance of viscous drag. To control the motion of the nano objects a continuous driving force and an external stimulus are necessary. The external stimulus may be in the form of light,[17–19] chemical gradient,[20–22] magnetic field,[23–25] electric field,[26,27] ultrasonic sound.[28] Depending on the interaction between the particle and the input energy source the movement can be translation,[29,30] rotation,[31] rolling,[32] contraction,[33] delivery[34] or collective motion.[35]

In the present work we have mainly focused on chemically propelled nanomotors. The motion of the chemical nanomotors can be explained by generation of surface tension gradients,[36] bubble propulsion,[37] osmosis[38] or self-electrophoresis.[39] Chemical propulsion depends on the chemical fuel used and till date the most extensively used chemical fuel is H_2O_2.[40,41] The shape[10] and symmetry[42] of the nanomotor also plays a vital role in determining the mechanism of the motion.

Soft state of oxometalates comprising of superstructures of oxometalates are known as soft-oxometalates (SOMs)[43–51] and since they are soft in nature they can be rendered motile deliberately using correct chemical fuel or by any other suitable external energy. We have already induced motion in SOMs using both physical as well as chemical external energy sources.[17,52] In one of our previous works mesoscopic asymmetric peapod shaped SOM's[50] controlled motion along complex paths using tailor-made sophisticated optical potentials was reported.[17] In another work motion was induced in heptamolybdate based SOMs using dithionite as a fuel from which SO_2 was generated to propel the SOMs.[52] As a next step we try to exploit the intrinsic acidity of the SOMs and propel them by exposing them to a bicarbonate rich environment which can

EFAML, Materials Science Centre, Department of Chemistry, Indian Institute of Science Education and Research, Kolkata-741246, India. E-mail: s.roy@iiserkol.ac.in

† Electronic supplementary information (ESI) available. See DOI: 10.1039/c6ra24132h

produce CO_2 which can propel the SOMs. The SOM used here as the nanomotor is composed of oxoanions of two metals – molybdenum and vanadium. The morphology of these SOMs can be tuned by varying the loading of the two metal oxoanions which helps us achieving control in the movement of the SOMs. As mentioned earlier, the primary design principle of the SOM nanomotors is based on the fact that the SOMs are heteropolyacids which evolve CO_2 (propelling the SOMs) from bicarbonate which is used as the fuel. Here we first describe its synthesis and characterization and later its motion.

Experimental

Materials and methods

All the reagents were purchased from commercial sources (Merck) and were used without further purification. The glassware were cleaned in an acid bath, base bath and then rinsed with isopropanol followed by acetone and kept in hot air oven for 48 hours prior use.

Synthesis of V/Mo soft-oxometalate (SOM)

Ammonium heptamolybdate tetrahydrate (800 mg, 0.687 mmol) was dissolved in distilled water (4 mL) and heated until simmering hot. A clear dispersion of ammonium heptamolybdate was formed which was kept in refrigerator for 10 minutes. This dispersion was then brought back to room temperature. To this solution a specific amount of sodium metavanadate was added separately to prepare dispersions such that the molar ratio of sodium metavanadate to ammonium heptamolybdate (V/Mo loading) were 0.08, 0.10, 0.12, 0.14, 0.17, 0.24, 0.50, 0.70 and 1.00 respectively. After addition of metavanadate the mixture was sonicated for 15 minutes using an ultrasonicator to form a stable dispersion. The dispersion was brought back to room temperature and kept undisturbed for 24 hours for equilibration. Beyond the V/Mo loading ratio of 0.50 precipitate was obtained after 24 hours.

Preparation of sodium bicarbonate solutions

Calculated amounts of sodium bicarbonate were dissolved in 10 mL of distilled water to prepare bicarbonate solutions of concentrations 0.0119 mol L^{-1}, 0.0238 mol L^{-1}, 0.0416 mol L^{-1}, 0.0595 mol L^{-1}, 0.0952 mol L^{-1}, 0.1190 mol L^{-1}, 0.1428 mol L^{-1}, 0.1785 mol L^{-1}, 0.2142 mol L^{-1}, 0.2381 mol L^{-1}, 0.2976 mol L^{-1}, which were used as fuels.

Instrumental analysis

Microscopy using inverted fluorescence microscope. An Olympus IX81 epi fluorescence microscope with a motorized stage was used for recording the videos of moving nanomotors. A 22 × 40 dimension glass cover slip was cleaned with methanol and dried in air to remove any unwanted adsorbed materials on the surface of the cover slip. The V/Mo SOM dispersion of varying V/Mo molar ratio (10 μL) was placed on the cover slip using a 10 μL micropipette. This coverslip was then placed on the scanning stage of the microscope and the stage was controlled using a joystick. The microscope was focused at objective 40× and the video of the SOM dispersion was recorded in order to locate the SOMs and this video acts as the control of the experiment. To this SOM dispersion, sodium bicarbonate solution (10 μL) was added using a 10 μL micropipette to ensure that 1 : 1 volume ratio is maintained. The microscope was again focused at objective 40× and the videos were recorded using DSIC camera attached with the microscope. This procedure was repeated 3 times each for all concentrations of sodium bicarbonate as well as for all variations of V/Mo loading to ensure the reproducibility of the process and to get more number of data points for analysis.

Characterizations using Scanning Electron Microscopy (SEM) and energy dispersive X-ray analysis (EDAX). The SEM and EDAX images of the SOM dispersions (with varying vanadate/molybdate loading) were recorded on SUPRA 55 VP-41-32 instrument with the SmartSEM version 5.05 Zeiss software and EDS Oxford software.

Characterizations using Dynamic Light Scattering (DLS) measurement. 1 mL of V/Mo SOM dispersion (of a particular V/Mo loading) was diluted with 10 mL of deionised water and this dispersion was subject to a hand-held laser pointer of wavelength 635 nm to ensure that the resulting scattering is a single well-defined line. The dispersion was then kept in a Malvern Zetasizer to confirm the size of the dispersed particles. The procedure was repeated for all variations of vanadate–heptamolybdate loadings.

Characterizations using Horizontal Attenuated Total Reflectance-Infra red (HATR-IR) spectroscopy. A Perkin-Elmer Spectrum RX1 spectrophotometer with HATR (Horizontal Attenuated Total Reflectance) facility in the range of 2000–600 cm^{-1} was used to record the HATR-IR spectrum of the SOM dispersion. The same set-up was also used to record the HATR-IR spectra of ammonium heptamolybdate and decavanadate to compare them with the spectrum of the V/Mo SOM.

Characterizations using Raman spectroscopy. Raman spectra were recorded for all variations of V/Mo loadings in SOMs as well as for heptamolybdate and decavanadate dispersions using commercial Raman spectromicrometer (Horiba Jobin Yvon LABRAM HR800). The excitation laser at 633 nm was shined on the dispersion kept in a quartz cuvette on the Raman microscope stage.

Characterization using powder X-ray diffraction (PXRD). The dispersion of SOM with 0.50 V/Mo loading was drop cast on a glass slide, dried in air and the sample was scratched out. The sample was subject to Rigaku (mini flex II, Japan) powder X-ray diffractometer having Cu Kα = 1.540593 Å radiation.

Analysis of motion of SOMs

Analysis using ImageJ. The raw microscopic image sequence in TIFF format was converted to AVI using a commercial image analysing software ImageJ at the rate of 10 frames per second as specified during recording of video. Each frame from the video was taken separately and analysed manually for SOM particles. The co-ordinates of all SOM particles in each frame were noted and each SOM particle was traced for 5 frames. The body length of that particular SOM was calculated from the co-ordinates,

time gap between the frames was noted and using all these information the velocity of the moving SOMs was calculated in terms of body lengths s^{-1}. This procedure was repeated for a number of SOMs to obtain the average velocity for each concentration of sodium bicarbonate solution. The same analysis was also used for the videos of varied V/Mo loadings. The velocities of the moving SOM were plotted in a graph against concentration of sodium bicarbonate. In another graph the velocity of the SOM was plotted against the composition *i.e.*; the ratio of vanadate to molybdate, or the V/Mo loading in SOMs.

Analysis using TrackPy. TrackPy[53] is a python packaging tool developed for particle tracking. Each video was analysed by writing a code in TrackPy to obtain the trajectories of the moving SOMs. Trackpy first identified the SOM particles in each frame with selective filters in it and then connected a definite number of frames in which a SOM particle was present following instructions to obtain the particle trajectories directly. For each sodium bicarbonate solution concentration codes were written separately and particle trajectories were obtained. The procedure was repeated for all V/Mo ratio variations of SOMs as well.

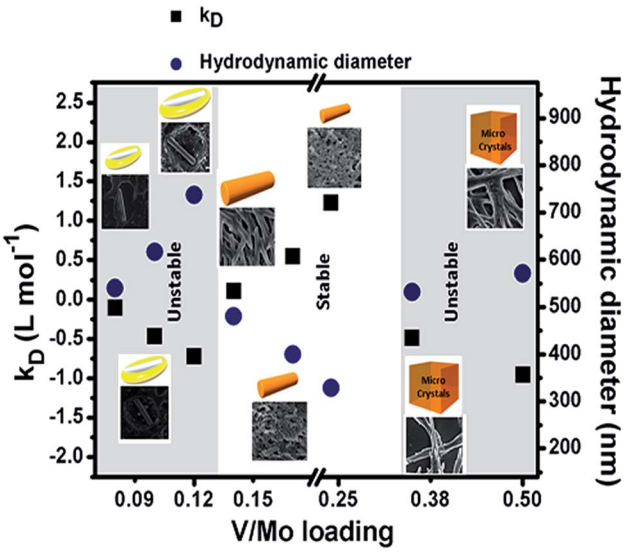

Fig. 1 Stability study of V/Mo SOMs at different loading of V/Mo from k_D value and hydrodynamic diameter obtained from DLS study.

Results and discussion

We first describe the formation of the vanadate–molybdate SOM and later its characterization with the help of Scanning Electron Microscopy (SEM), Energy Dispersive X-ray Analysis (EDAX), Dynamic Light Scattering (DLS), Powder X-ray Diffraction (PXRD), Horizontal Attenuated Total Reflectance-Infra Red (HATR-IR) Spectroscopy and Raman spectroscopy.

Different morphologically distinctive aqueous dispersions of SOMs are made from the initial dispersion of heptamolybdate in water[52] and sodium metavanadate, by suitably adjusting the molar ratio of vanadate and molybdate (V/Mo loading = 0.08, 0.10, 0.12, 0.14, 0.17, 0.24, 0.35 and 0.50) followed by sonication for 15 minutes and thermal equilibration at 25 °C for another 24 hours.

We first check the stability of the dispersions. To do so, we employed the relation $D = D_0(1 + k_D C)$ where D = diffusion coefficient measured from hydrodynamic radii (from DLS), D_0 = diffusion coefficient at zero concentration, C = sample concentration in mol L^{-1}, k_D is a complex function depending on hydrodynamic radii which predicts the repulsive electrostatic interactions among SOMs.[54] The positive value of k_D confirms the stability of the SOMs, with increasing negative value of k_D the SOMs become unstable. From the k_D *vs.* V/Mo loading graph (Fig. 1) dispersions with V/Mo loading of 0.14, 0.17 and 0.24 are found to be more stable than others. DLS size distribution experiments (Fig. S1†) show that for V/Mo loading of 0.08 to 0.12 the average hydrodynamic diameter (D_h) of SOMs vary from 500–740 nm (Fig. 1) and from SEM we observe that in such SOMs the rods of $\{Mo_7\}$ are nested within the cavity of vanadate. With further increase in vanadate concentration, *i.e.*; for V/Mo loading of 0.14–0.24 there is a morphological transformation back to nanorods, with hydrodynamic diameter decreasing to 330 nm as evident from Fig. 1. At and beyond V/Mo loading of 0.35 the system becomes unstable and microcrystalline sharp needles (Fig. 2) of vanadate–molybdate precipitate. The graph in Fig. 2 compares the experimental loading of V/Mo ratios in the SOMs with the ratios obtained from EDAX mapping (Fig. S2†). The V/Mo ratios obtained from EDAX are slightly less than the experimental loading ratios but it follows the same trend as the experimental ones.

We now speculate on the reasons for obtaining various morphologies in the dispersions. Dispersing ammonium heptamolybdate (0.687 mmol) in 4 mL of water gives rise to a pH of 5.5. Vanadate in between pH range of 4–9 exists as decavanadate.[55] Hence, all the above morphologies are created by self-assembly of heptamolybdate and decavanadate which we have confirmed from HATR-IR later. Though the exact structure of the $(Mo_7–V_{10})$ based SOMs cannot be obtained we provide a model of the formation of the SOMs from the constituent polyoxometalates–heptamolybdate and decavanadate *via* hydrogen bonding (Fig. 3). The above mentioned SOMs have been synthesized *via* sonication which is a versatile technique for creating nanostructures. Ultrasonic waves generate hollow structures *via* subsequent generation, growth and collapse of bubbles in aqueous solution.[56] These bubbles create a liquid–air interface which acts as a template for the growth of hollow spherical vanadate SOMs.[57] Heptamolybdate rods have higher surface energy than vanadate spheres as spheres are the lowest energy structures. We believe that to minimise the magnitude of electrostatic repulsion between the heptamolybdate rods they take shelter within the vanadate cavity which is responsible for the embedded morphologies of rods in shells for the V/Mo loadings of 0.08, 0.10 and 0.12.[58] Till now this system is under thermodynamic control, on addition of further electrolyte in the form of sodium metavanadate the spheres get transformed to $\{Mo_7–V_{10}\}$ rods. For V/Mo loadings higher than 0.12 we believe the added electrolyte minimizes the electrostatic repulsion thus stabilizing the kinetically controlled rods and k_D values are

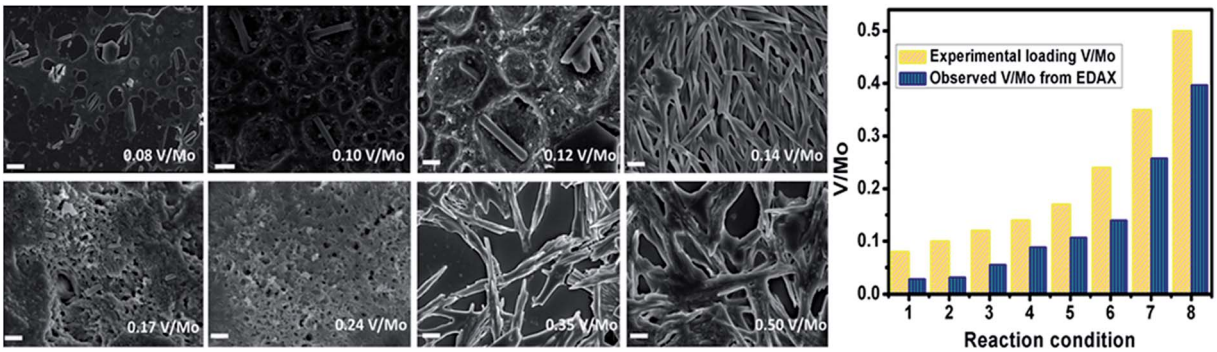

Fig. 2 Scanning Electron Microscopy (SEM) images of molybdenum/vanadium SOM at varying V/Mo ratio. Scale bar 200 nm. The graph indicates the molar ratio of V/Mo and the observed V/Mo from EDAX. Reaction conditions are indicated by (1) 0.08 V/Mo, (2) 0.10 V/Mo, (3) 0.12 V/Mo, (4) 0.14 V/Mo, (5) 0.17 V/Mo, (6) 0.24 V/Mo, (7) 0.35 V/Mo and (8) 0.50 V/Mo (experimental molar ratio of loading).

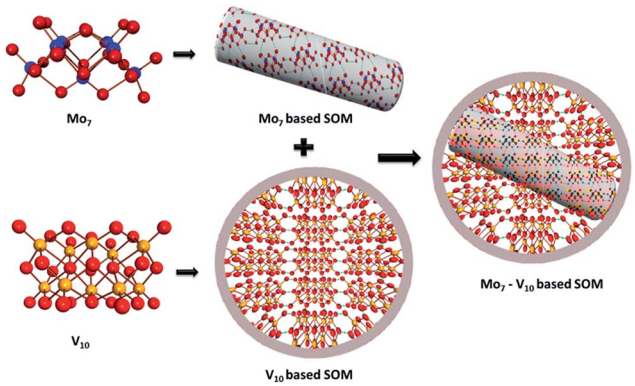

Fig. 3 Schematic showing the probable model of (Mo_7–V_{10}) SOMs formed the constituent POMs: (Mo_7) and (V_{10}). Color code: Mo (blue ball), V (yellow ball), O (red ball), hydrogen bonding (green dotted lines).

positive implying stability of SOMs.[59] Finally for V/Mo ratios beyond 0.24 the system becomes unstable again and it flocculates in the form of microcrystals, which we have further investigated with powder X-ray diffraction (PXRD) (Fig. 4).

Fig. 4 shows the powder X-ray diffraction (PXRD) pattern of vanadate–molybdate composite with intense peaks centered at 8.5290, 10.2060, 11.1330, 13.2360, 15.1780, 23.0000, 29.9160, 34.4610 with *d*-spacings of 1.036, 0.866, 0.794, 0.668, 0.583, 0.386, 0.298, 0.260 nm respectively. The peaks at 15.1780, 23.0000, 34.4610 may be assigned to the Bragg's reflections from (006), (009), (0012) planes of decavanadate respectively.[60] The peaks at 8.5290, 10.2060, 11.1330, 13.2360, 29.9160 may be from [(011), (040)], [(100), (110)], (−121), [(041), (130)], (023) planes of heptamolybdate respectively.[61] The peaks are broadened due to the formation of micron sized crystals. In this process of composite formation, lattices of both the oxoanions do not remain intact which could be clearly understood from the change in the *d* values as compared to literature.[60,61] A new lattice might have been formed in the process with probable interpenetration of the vanadate and molybdate lattices, exact structure of which is beyond the scope of this paper.

In order to confirm that the SOM is composed of vanadate–molybdate we have characterized the heptamolybdate dispersion, decavanadate dispersion and the SOM dispersion by HATR-IR spectroscopy. From the HATR-IR spectra (Fig. 5) we have observed characteristic peaks of ammonium heptamolybdate tetrahydrate at 1634 cm^{-1} due to stretching of O–H bond. The peak at 1402 cm^{-1} is due to bending of N–H bond of the ammonium ion and the peaks at 895 cm^{-1} and 841 cm^{-1} are due to symmetric and asymmetric stretching modes of the vibration in MoO_4^{2-}. For decavanadate the peaks were observed at 1634 cm^{-1} for symmetric stretching of O–H bond, at 962 cm^{-1} and 841 cm^{-1} for symmetric and asymmetric stretching vibrations of V=O bond. For the SOM dispersion, peaks were observed at 1639 cm^{-1} for O–H bond stretching, 1402 cm^{-1} for N–H bending, 890 cm^{-1} and 841 cm^{-1} for symmetric and asymmetric Mo=O stretching, 949 cm^{-1} and 841 cm^{-1} for symmetric and asymmetric stretching vibrations of V=O bond. We observe a shift in O–H bond stretching for the SOM dispersion which is due to hydrogen bonding type interaction between the interacting vanadate and molybdate clusters. Shifts in Mo=O and V=O stretching vibrations indicate weak

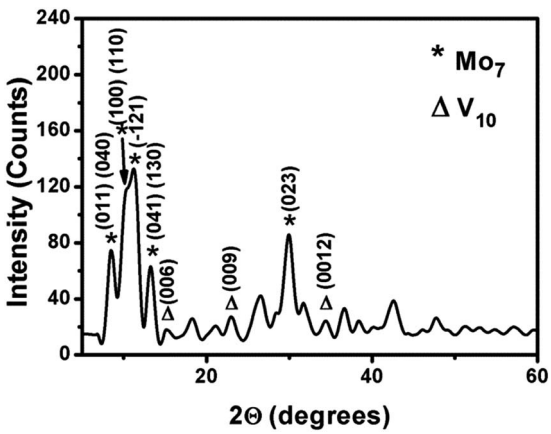

Fig. 4 Powder XRD of the V/Mo composite at molar ratio of 0.35. The peaks with * represent the planes of {Mo_7} and those with Δ represent the planes of {V_{10}}.

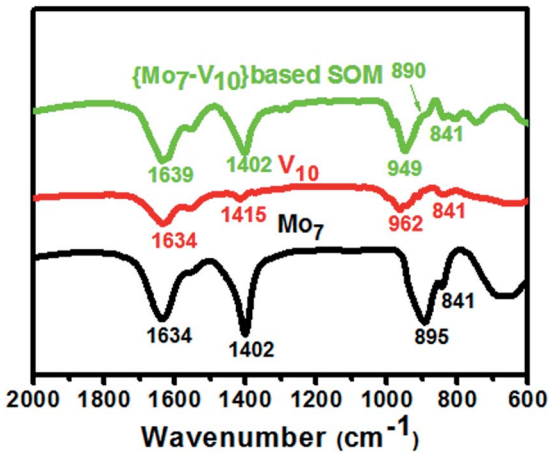

Fig. 5 HATR-IR spectra of heptamolybdate (Mo_7), decavanadate (V_{10}) and (Mo_7–V_{10}) based SOM.

interactions between molybdate and vanadate. From these peaks we infer that the SOM is indeed composed of vanadate and molybdate.

From Raman spectroscopy (Fig. 6) we observe that decavanadate is Raman inactive. $\{Mo_7\}$ alone possesses Raman bands at 944, 918, 590, 365 and 214 cm^{-1} which may be attributed to Mo=O symmetric and asymmetric stretching vibrations, Mo–O–Mo symmetric stretching (weak band), Mo=O bending and Mo–O–Mo deformations respectively. In case of SOMs with different V/Mo loading the Raman bands are shifted to 938, 894, 360 and 212 cm^{-1}. This shift to lower wavenumbers may be due to higher polarizability of the bonds as they are attached to oxoanions of vanadium.

We now analyze the morphologies obtained for V/Mo loadings of 0.08 to 0.12. We observe for V/Mo loading of 0.08 to 0.12 a structure of a rod nested within a hollow cavity. To prove the nanorods are of heptamolybdate and the cavity consists of vanadate we varied the energy density of the probing electron beam in the scanning electron microscope. This is done by increasing the accelerating voltage from 7–17 kV while

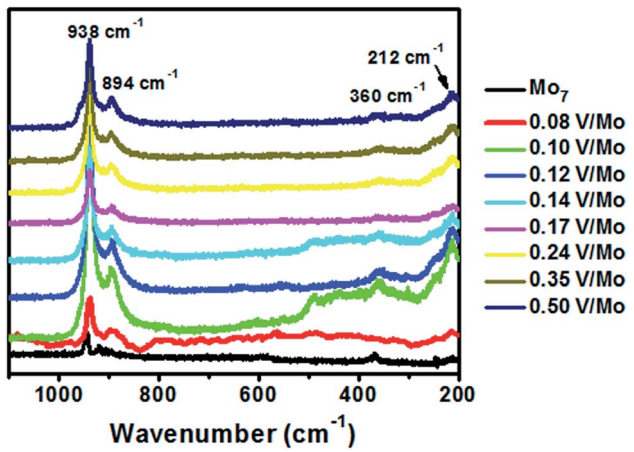

Fig. 6 Raman spectra of heptamolybdate SOM and V/Mo SOMs at their various loading values.

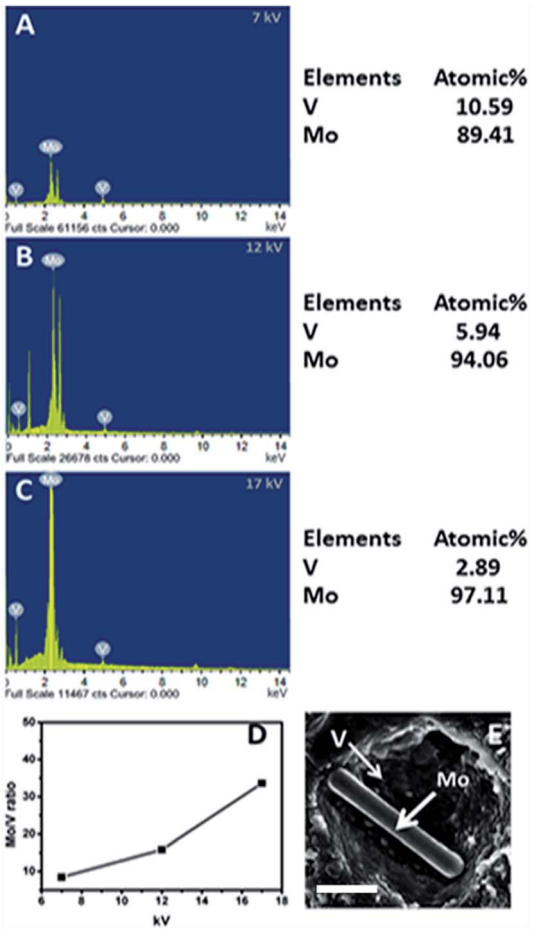

Fig. 7 EDAX spectra of the V/Mo SOMs at (A) 7, (B) 12 and (C) 17 kV. (D) Plot of V/Mo ratio against the accelerating voltage of the electron beam. (E) SEM image of SOM for V/Mo loading of 0.08 where $\{Mo_7\}$ rich nanorod is present within a cavity rich with vanadates. Scale bar: 200 nm.

performing energy dispersive X-ray analysis (Fig. 7). Mo/V ratio is measured at a particular location and it is observed that on accelerating energy the Mo/V ratio also increases from 8.44 to 33.60. This is because at lower energy density the electron beam can penetrate only up to a few layers while higher energy beam penetrates deep inside the cavity. This shows that the surface of the structure is rich in vanadates while deeper structure where rod is present is rich in molybdates. This clearly shows that $\{Mo_7\}$ rich rods are cradled inside the cavities rich in vanadates.

Now we investigate the motion of SOMs with varying V/Mo loading and for different concentrations of fuel. As mentioned earlier, in this paper these SOMs are used as the nanomotors and an aqueous solution of sodium bicarbonate is used as the fuel. The dispersion of heptamolybdate SOMs (*i.e.*, V/Mo loading of 0) is found to be acidic with a pH of 5.5. These heteroacid SOMs evolve CO_2 from bicarbonate solution according to the following reactions:

$$HCO_3^- + H^+ (SOM) \rightarrow H_2CO_3$$

$$H_2CO_3 \rightarrow H_2O + CO_2 (g)\uparrow$$

Even though evolution of CO_2 is observed from the heptamolybdate SOM dispersion, these SOMs alone do not exhibit any autonomous motion. We believe that due to absence of any anisotropy in the structure of these SOMs, the evolution of CO_2 is non-directional and symmetric and hence it cannot induce motion. So we ask – can some asymmetry be induced in these particles to make them active as anisotropy plays a crucial role in the movement of active nanomotors? On introduction of vanadate in the molybdate SOMs *i.e.*; with varying V/Mo loading the desired anisotropy is obtained which in turn renders motility in these nanoparticles. However, for only vanadate containing SOM dispersion no effervescence is observed on addition of bicarbonate solution. Hence it may be inferred that the carbon dioxide is generated from the molybdate part of the SOMs and the motility is induced due to asymmetry introduced in these SOMs by the vanadates.

To elucidate the motion of the SOMs qualitatively we propose that a mobile diffused boundary is generated between the starting SOM and the species generated after reaction. This interface in turn generates an osmotic boundary where CO_2 gas is produced which again gives rise to a slip velocity between the SOM surface and the continuous medium.

To interpret the effect of the fuel on the mechanism of motion we varied the loading of concentration of the fuel on a given SOM dispersion with a fixed V/Mo loading of 0.17. It is observed that the propulsion velocity of these SOMs increases with increasing concentration of the fuel which is obvious as more and more CO_2 is generated that amplifies the chemical potential gradient near the SOM surface leading to greater propulsion. The propulsion velocity reaches a maximum of 72 body lengths s^{-1} at 0.0595 mol L^{-1} of sodium bicarbonate concentration. After the tipping point and past this fuel concentration, the propulsion diminishes (Fig. 8A). This is due to the fact that some CO_2 gets adsorbed on the free SOM surface thereby saturating the reaction sites which exerts an additional viscous drag on the SOMs.

Consequently, the velocity of the SOMs dwindles even though we increase the concentration of the fuel. To analyse the individual movement of each SOM particle we have calculated the velocity of the SOM at different concentrations of bicarbonate (Fig. 8A) and shown the time lapse images of the moving SOM in 0.0595 mol L^{-1} bicarbonate solution.

Now to perceive the impact of asymmetry on actuation of these nanomotors eight SOM dispersions were prepared by altering the loading of V/Mo (Fig. 9A). For the first dispersion having an interpenetrating rod encapsulated in a shell of vanadate where V/Mo loading was 0.08 the mean propulsion velocity was found to be 40 body lengths s^{-1} (Fig. 9A). We have also obtained the trajectories of the motile SOMs for time duration of 1 second with ImageJ and TrackPy (Fig. 9B).

The coloured lines indicate the distance travelled by each SOM for 1 second in bicarbonate solutions.

With increase in vanadate loading in the SOM (for V/Mo loading of 0.08 to 0.12) the extent of encapsulation of molybdate by vanadate increases thereby decreasing the interaction between the heptamolybdate rods and the bicarbonate solution. Hence less CO_2 is produced and the propulsion velocities of the SOMs reduce till V/Mo loading reaches 0.12. Now for V/Mo loading of 0.14 to 0.24 the encapsulation of molybdate by vanadate is not seen anymore.

Instead we see only nanorods that are chemically anisotropic and are composed of both vanadate and molybdate. Hence for SOMs with V/Mo loading of 0.14 and above the bicarbonate solution can directly interact with the molybdate present in the nanorods with vanadate imparting asymmetry thereby enhancing the propulsion velocity. For 0.17 and 0.24 loading of V/Mo, the size of the nanorods diminishes ensuing acceleration of the SOMs. For SOMs with V/Mo loading of 0.35 and 0.50 microcrystalline rods of increasing size are produced and consequently the velocity drops again. Beyond the V/Mo loading of 0.5 the dispersion of V/Mo SOM becomes unstable. Now we discuss the effect of size on the propulsion velocity of mixed vanadate–molybdate SOMs. For the vanadate encapsulated molybdate rods at V/Mo loading of 0.12 the hydrodynamic

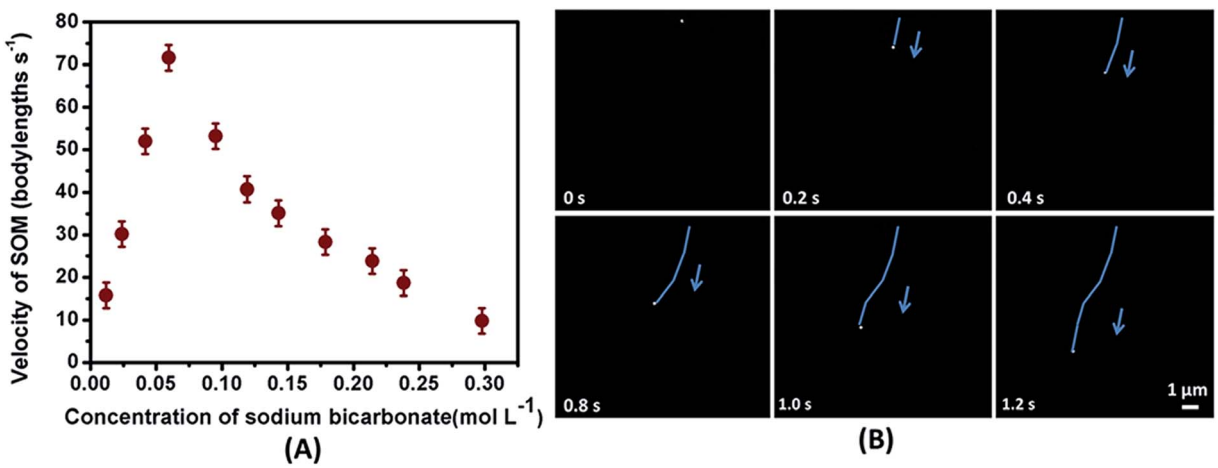

Fig. 8 (A) Plot of velocity of SOMs (0.17 V/Mo loading) at various concentrations of $NaHCO_3$. (B) Time lapse images of autonomously moving SOM particle in 0.0595 mol L^{-1} $NaHCO_3$ solution. The blue arrows show the direction of motion of the SOMs.

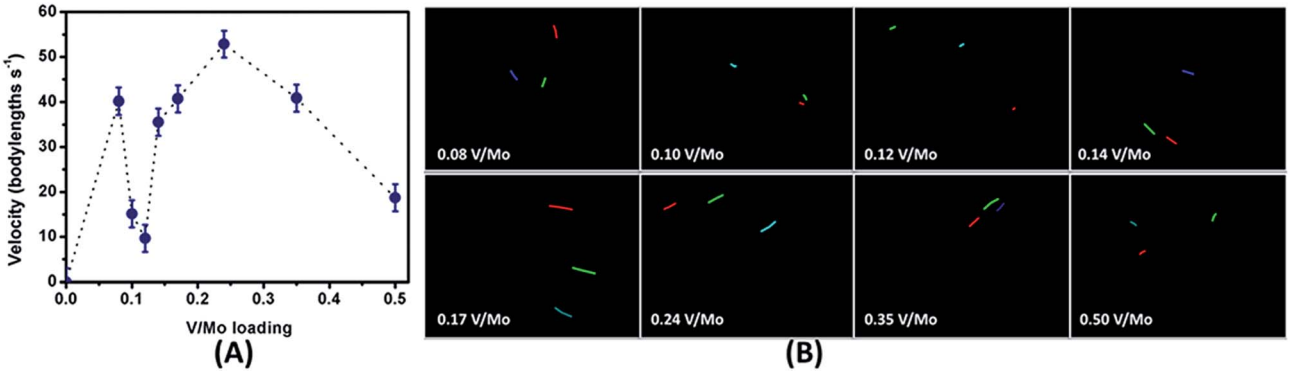

Fig. 9 (A) Plot of velocity of SOMs by varying V/Mo loading. (B) Trajectories of the moving SOMs as obtained from TrackPy for a time duration of 1 second. The coloured lines show the trajectories for different SOM particles.

diameter is 740 nm and the propulsion velocity is the lowest ~9 body lengths s^{-1}. For the vanadate–molybdate rods at V/Mo loading of 0.24 the hydrodynamic diameter reduces to 330 nm and the velocity is the highest *i.e.*; 53 body lengths s^{-1}. It is also to be noted that in low Reynold's number regime, the axial propulsion force of the nanomotors calculated by Stokes' equation is compensated by the drag force of the fluid on the nanomotors.[62,63] For the nanorod encapsulating vesicular SOMs the drag force is (0.285 ± 0.012) fN while for the rod-like SOMs it is (0.736 ± 0.009) fN which explains the higher propulsion velocity of the rod-like SOMs.

So the following points emerge from our study:

(1) Although molybdate is responsible for effervescence of CO_2 from bicarbonate, alone molybdate based SOMs cannot show motility when treated with fuel bicarbonate. Instead induction of chemical anisotropy in the form of mixed metalate SOM with V and Mo is required for observing motility.

(2) However for a SOM with chemical anisotropy, *i.e.*, SOMs with vanadate and molybdate, the hydrodynamic radius of the SOM inversely influences the velocity of propagation. It is observed that smaller the hydrodynamic radius, higher is the velocity of the SOM.

From all the above results we thus infer that the autonomous motion of the nanomotors is dependent on the anisotropy of SOMs, and the size of the individual nanomotors, for a given concentration of the fuel.

Conclusions

To summarize, in this work we have reported a decavanadate and heptamolybdate based soft-oxometalate (SOM) system and employed sodium bicarbonate solution as fuel to render these nano particles motile. The decomposition of bicarbonate to form CO_2 in the presence of acidic dispersion of heptamolybdate is the driving force behind the motion of the SOMs. Vanadate induces asymmetry in these SOMs which provides directionality to the translation. In this work we have clearly demonstrated that size and chemical anisotropy of SOMs play a crucial role in their movement which is reflected in the magnitude of their propulsion velocity. Thus we can tune the movement of the SOMs either by controlling their size or by varying the molar ratio of the chemical constituents – vanadate and molybdate and hence possibilities exist for controlling their motion and using them as devices for transport and delivery.[64–66]

Acknowledgements

SR gratefully acknowledges the grants from IISER-Kolkata, India, DST-fast track, BRNS-DAE grant.

Notes and references

1 J. Wang, *Nanomachines: fundamentals and applications*, John Wiley & Sons, 2013.
2 J. Wang, *Lab Chip*, 2012, **12**, 1944–1950.
3 J. Li, W. Gao, R. Dong, A. Pei, S. Sattayasamitsathit and J. Wang, *Nat. Commun.*, 2014, **5**, 5026.
4 K. Kim, X. Xu, J. Guo and D. Fan, *Nat. Commun.*, 2014, **5**, 3632.
5 R. D. Vale and R. A. Milligan, *Science*, 2000, **288**, 88–95.
6 A. Upadhyaya and A. van Oudenaarden, *Curr. Biol.*, 2003, **13**, R734–R744.
7 G. Woehlke and M. Schliwa, *Nat. Rev. Mol. Cell Biol.*, 2000, **1**, 50–58.
8 H. Yin, M. D. Wang, K. Svoboda and R. Landick, *Science*, 1995, **270**, 1653.
9 R. F. Ismagilov, A. Schwartz, N. Bowden and G. M. Whitesides, *Angew. Chem., Int. Ed.*, 2002, **41**, 652–654.
10 W. F. Paxton, K. C. Kistler, C. C. Olmeda, A. Sen, S. K. S. Angelo, Y. Cao, T. E. Mallouk, P. E. Lammert and V. H. Crespi, *J. Am. Chem. Soc*, 2004, **126**, 13424–13431.
11 S. Fournier-Bidoz, A. C. Arsenault, I. Manners and G. A. Ozin, *Chem. Commun.*, 2005, **4**, 441–443.
12 P. Fischer and A. Ghosh, *Nanoscale*, 2011, **3**, 557–563.
13 T. R. Kline, W. F. Paxton, T. E. Mallouk and A. Sen, *Angew. Chem., Int. Ed.*, 2005, **44**, 744–746.
14 M. Guix, C. C. Mayorga-Martinez and A. Merkoçi, *Chem. Rev.*, 2014, **114**, 6285–6322.
15 S. Nakata, Y. Doi and H. Kitahata, *J. Colloid Interface Sci.*, 2004, **279**, 503–508.

16 G. Zhao, T. H. Seah and M. Pumera, *Chem.–Eur. J.*, 2011, **17**, 12020–12026.
17 B. Roy, N. Ghosh, P. K. Panigrahi, A. Banerjee, A. Sahasrabudhe, B. Parasar and S. Roy, *J. Mol. Eng. Mater.*, 2014, **2**, 1440006.
18 W. Duan, M. Ibele, R. Liu and A. Sen, *Eur. Phys. J. E: Soft Matter Biol. Phys.*, 2012, **35**, 1–8.
19 Y. Li, F. Mou, C. Chen, M. You, Y. Yin, L. Xu and J. Guan, *RSC Adv.*, 2016, **6**, 10697–10703.
20 W. Gao, S. Sattayasamitsathit, J. Orozco and J. Wang, *J. Am. Chem. Soc*, 2011, **133**, 11862–11864.
21 N. S. Zacharia, Z. S. Sadeq and G. A. Ozin, *Chem. Commun.*, 2009, **39**, 5856–5858.
22 Q. Xiao, J. Li, J. Han, K.-X. Xu, Z.-X. Huang, J. Hu and J.-J. Sun, *RSC Adv.*, 2015, **5**, 71139–71143.
23 L. Zhang, T. Petit, Y. Lu, B. E. Kratochvil, K. E. Peyer, R. Pei, J. Lou and B. J. Nelson, *ACS Nano*, 2010, **4**, 6228–6234.
24 S. Tottori, L. Zhang, F. Qiu, K. K. Krawczyk, A. Franco-Obregón and B. J. Nelson, *Adv. Mater.*, 2012, **24**, 811–816.
25 I. Kavre, G. Kostevc, S. Kralj, A. Vilfan and D. Babič, *RSC Adv.*, 2014, **4**, 38316–38322.
26 S. T. Chang, V. N. Paunov, D. N. Petsev and O. D. Velev, *Nat. Mater.*, 2007, **6**, 235–240.
27 G. Loget and A. Kuhn, *J. Am. Chem. Soc*, 2010, **132**, 15918–15919.
28 V. Garcia-Gradilla, J. Orozco, S. Sattayasamitsathit, F. Soto, F. Kuralay, A. Pourazary, A. Katzenberg, W. Gao, Y. Shen and J. Wang, *ACS Nano*, 2013, **7**, 9232–9240.
29 C. Stock, N. Heureux, W. R. Browne and B. L. Feringa, *Chem.–Eur. J.*, 2008, **14**, 3146–3153.
30 M. Manjare, B. Yang and Y.-P. Zhao, *Phys. Rev. Lett.*, 2012, **109**, 128305.
31 J. Gibbs and Y. P. Zhao, *Small*, 2009, **5**, 2304–2308.
32 Y. He, J. Wu and Y. Zhao, *Nano Lett.*, 2007, **7**, 1369–1375.
33 J. C. Nawroth, H. Lee, A. W. Feinberg, C. M. Ripplinger, M. L. McCain, A. Grosberg, J. O. Dabiri and K. K. Parker, *Nat. Biotechnol.*, 2012, **30**, 792–797.
34 D. Kagan, R. Laocharoensuk, M. Zimmerman, C. Clawson, S. Balasubramanian, D. Kang, D. Bishop, S. Sattayasamitsathit, L. Zhang and J. Wang, *Small*, 2010, **6**, 2741–2747.
35 J. Berna, D. A. Leigh, M. Lubomska, S. M. Mendoza, E. M. Pérez, P. Rudolf, G. Teobaldi and F. Zerbetto, *Nat. Mater.*, 2005, **4**, 704–710.
36 H. Zhang, W. Duan, L. Liu and A. Sen, *J. Am. Chem. Soc*, 2013, **135**, 15734–15737.
37 A. A. Solovev, S. Sanchez, M. Pumera, Y. F. Mei and O. G. Schmidt, *Adv. Funct. Mater.*, 2010, **20**, 2430–2435.
38 W. Gao, A. Pei, R. Dong and J. Wang, *J. Am. Chem. Soc*, 2014, **136**, 2276–2279.
39 Y. Wang, R. M. Hernandez, D. J. Bartlett, J. M. Bingham, T. R. Kline, A. Sen and T. E. Mallouk, *Langmuir*, 2006, **22**, 10451–10456.
40 A. Agrawal, K. K. Dey, A. Paul, S. Basu and A. Chattopadhyay, *J. Phys. Chem. C*, 2008, **112**, 2797–2801.
41 J. Gibbs and Y.-P. Zhao, *Appl. Phys. Lett.*, 2009, **94**, 163104.
42 J. R. Howse, R. A. Jones, A. J. Ryan, T. Gough, R. Vafabakhsh and R. Golestanian, *Phys. Rev. Lett.*, 2007, **99**, 048102.
43 S. Roy, *Comments Inorg. Chem.*, 2011, **32**, 113–126.
44 S. Roy, *CrystEngComm*, 2014, **16**, 4667–4676.
45 B. Roy, M. Arya, P. Thomas, J. K. Jurgschat, K. Venkata Rao, A. Banerjee, C. Malla Reddy and S. Roy, *Langmuir*, 2013, **29**, 14733–14742.
46 S. Das, P. Thomas and S. Roy, *Eur. J. Inorg. Chem.*, 2014, **2014**, 4551–4557.
47 P. Thomas, C. Pei, B. Roy, S. Ghosh, S. Das, A. Banerjee, T. Ben, S. Qiu and S. Roy, *J. Mater. Chem. A*, 2015, **3**, 1431–1441.
48 K. Das and S. Roy, *Chem.–Asian J.*, 2015, **10**, 1884–1891.
49 S. Das, S. Biswas, T. Balaraju, S. Barman, R. Pochamoni and S. Roy, *J. Mater. Chem. A*, 2016, **4**, 8875.
50 S. Roy, M. T. Rijneveld-Ockers, J. Groenewold, B. W. Kuipers, H. Meeldijk and W. K. Kegel, *Langmuir*, 2007, **23**, 5292–5295.
51 S. Roy, L. C. Bossers, H. J. Meeldijk, B. W. Kuipers and W. K. Kegel, *Langmuir*, 2008, **24**, 666–669.
52 A. Mallick, D. Lai and S. Roy, *New J. Chem.*, 2016, **40**, 1057–1062.
53 D. Allan, T. Caswell, N. Keim and C. van der Wel, *TrackPy v0.3.2*, 2016.
54 M. Anyfantakis, A. Bourlinos, D. Vlassopoulos, G. Fytas, E. Giannelis and S. K. Kumar, *Soft Matter*, 2009, **5**, 4256–4265.
55 N. Greenwood and A. Earnshaw, *Chemistry of the Elements*, Butterworth-Heinemann, 2nd edn, 1997.
56 R. K. Rana, Y. Mastai and A. Gedanken, *Adv. Mater.*, 2002, **14**, 1414–1418.
57 C. Deng, H. Hu, X. Ge, C. Han, D. Zhao and G. Shao, *Ultrason. Sonochem.*, 2011, **18**, 932–937.
58 L. Zhang, K. Yu and A. Eisenberg, *Science*, 1996, **272**, 1777.
59 L. Zhang and A. Eisenberg, *Macromolecules*, 1996, **29**, 8805–8815.
60 R. G. Buchheit, H. Guan, S. Mahajanam and F. Wong, *Prog. Org. Coat.*, 2003, **47**, 174–182.
61 J. Wienold, R. E. Jentoft and T. Ressler, *Eur. J. Inorg. Chem.*, 2003, **2003**, 1058–1071.
62 T. Ui, R. Hussey and R. Roger, *Phys. Fluids*, 1984, **27**, 787–795.
63 S. Gilder and J. Glen, *Science*, 1998, **279**, 72–74.
64 S. Ebbens, R. A. Jones, A. J. Ryan, R. Golestanian and J. R. Howse, *Phys. Rev. E: Stat., Nonlinear, Soft Matter Phys.*, 2010, **82**, 015304.
65 L. Baraban, D. Makarov, R. Streubel, I. Mönch, D. Grimm, S. Sanchez and O. G. Schmidt, *ACS Nano*, 2012, **6**, 3383–3389.
66 L. L. del Mercato, M. Carraro, A. Zizzari, M. Bianco, R. Miglietta, V. Arima, I. Viola, C. Nobile, A. Sorarù and D. Vilona, *Chem.–Eur. J.*, 2014, **20**, 10910–10914.